

Nanoscale

Accepted Manuscript



This is an *Accepted Manuscript*, which has been through the Royal Society of Chemistry peer review process and has been accepted for publication.

Accepted Manuscripts are published online shortly after acceptance, before technical editing, formatting and proof reading. Using this free service, authors can make their results available to the community, in citable form, before we publish the edited article. We will replace this *Accepted Manuscript* with the edited and formatted *Advance Article* as soon as it is available.

You can find more information about *Accepted Manuscripts* in the [Information for Authors](#).

Please note that technical editing may introduce minor changes to the text and/or graphics, which may alter content. The journal's standard [Terms & Conditions](#) and the [Ethical guidelines](#) still apply. In no event shall the Royal Society of Chemistry be held responsible for any errors or omissions in this *Accepted Manuscript* or any consequences arising from the use of any information it contains.

Elastic Properties of Van Der Waals Epitaxy Grown Bismuth Telluride 2D Nanosheets

Lingling Guo,^{1,2} Haoming Yan,^{1,2} Quentarius Moore,³ Michael Buettner,² Jinhui Song,^{2,4} Lin Li,^{2,4} Paulo T. Araujo,^{2,5} and Hung-Ta Wang^{1,2,*}

¹Department of Chemical and Biological Engineering, The University of Alabama, Tuscaloosa, AL 35487, USA

²Center for Materials for Information Technology (MINT Center), The University of Alabama, Tuscaloosa, AL 35487, USA

³Department of Chemistry and Biochemistry, Jackson State University, Jackson, MS 39217, USA

⁴Department of Metallurgical and Materials Engineering, The University of Alabama, Tuscaloosa, AL 35487, USA

⁵Department of Physics and Astronomy, The University of Alabama, Tuscaloosa, AL 35487, USA

* Author to whom correspondence should be addressed. Electronic mail: htwang@eng.ua.edu

Abstract

Bismuth telluride (Bi_2Te_3) two-dimensional (2D) nanosheets prepared by van der Waals epitaxy were successfully detached, transferred, and suspended for nano-indentation measurements to be performed on freestanding circular nanosheets. The Young's modulus acquired by fitting linear elastic behaviors of 26 samples (thickness: 5~14 nm) is only 11.7~25.7 GPa, significantly smaller than the bulk in-plane Young's modulus (50~55 GPa). Compliant and robust Bi_2Te_3 2D nanosheets suggest the feasibility of the elastic strain engineering of topological surface states. (Total: 75 words)

Keywords: Bismuth telluride, 2D nanosheet, topological insulator, Young's modulus, mechanical properties.

Introduction

Bismuth telluride (Bi_2Te_3), bismuth selenide (Bi_2Se_3), and antimony telluride (Sb_2Te_3) are not only well-known thermoelectric materials, but also emerging topological insulator (TI) materials.¹⁻³ Unique topological surface states (TSSs) arise from a strong spin-orbit coupling, and these quantum states exist only on the surfaces of TIs. Likewise the electronic dispersion of graphene,⁴ the electronic dispersion of TI materials is described by the relativistic Dirac equation, which brings the electronic energies scaling linearly with the electronic momenta (*i.e.*, Dirac cone). The TSSs are spin-selective and are also protected against impurities and structural defects, which results in dissipation-less (*i.e.*, ballistic) electronic transport. This provides opportunities for revolutionizing many energy-related technologies, such as thermoelectric modules, infrared detectors, and heterogeneous catalysis.⁵ One of major challenges in the application of TSSs is the lack of approaches to open a bandgap at the Dirac cone and to tune the TSS bandgap once it's successfully opened.

Recent TI research activities have successfully demonstrated bandgaps of TSSs by hybridizing TSSs at the top and the bottom surface of a nanofilm, as its thickness is below the TSS penetration depth (*i.e.*, 5 nm for Bi_2Te_3).^{6,7} Unfortunately, TSS bandgaps obtained by the thickness-controlled hybridization could not be tuned, which will limit TSSs' application potential. Using two-dimensional (2D) nanosheets, elastic strain engineering is an attractive method for opening and tuning TSS bandgaps based on two main reasons; firstly, Bi_2Te_3 is one of van der Waals layered materials, and elastic deformations can be easily induced in 2D nanosheets. Secondly, theories have shown that elastic strain engineering is promising for tuning TSSs' bandgap in a TI material.^{8,9} Such strain-dependent electronic bandgaps have also been demonstrated in graphene¹⁰⁻¹² and molybdenum disulfide (MoS_2) 2D nanosheets,^{13,14} because

elastic strains could be robustly induced in graphene ($\sim 10\%$)¹⁵ and MoS₂ 2D nanosheets (6~11%).¹⁶⁻¹⁹

The Bi₂Te₃ monolayer, often called quintuple layer (QL), has a thickness of ~ 1 nm, which consists of five atomic layers covalently bonded in the sequence of Te-Bi-Te-Bi-Te along the *c*-axis of the rhombohedral crystal.² The crystal of bulk Bi₂Te₃ is a stack of QLs, in which adjacent QLs are held together by weak van der Waals interactions. Owing to the unique crystal anisotropy, Bi₂Te₃ multi-QL 2D nanosheets could be prepared using either top-down exfoliations (*i.e.*, breaking van der Waals bonding),²⁰ or bottom-up syntheses (*i.e.*, van der Waals epitaxy).²¹ Understanding elastic properties of Bi₂Te₃ 2D nanosheets has become an imperative topic for exploring strain-controlled electronic transport in TSSs.

To aid in understanding elastic properties of Bi₂Te₃ 2D nanosheets, we performed atomic force microscope (AFM) based nano-indentations¹⁵ to test mechanical properties of suspended Bi₂Te₃ 2D nanosheets containing 5~14 QLs (thickness: 5~14 nm). Elastic behaviors, Young's modulus, and the pretension of 5~14 QL nanosheets were obtained by fitting the thickness-dependent linear elastic behavior using Komaragiri *et al.*'s model,²² which is a previously demonstrated method for characterizing multi-layered 2D nanosheets of MoS₂ and mica.^{17, 23}

Experimental

Owing to an excellent thickness control, Li *et al.*'s van der Waals epitaxy²¹ was used to prepare Bi₂Te₃ 2D nanosheets for this study. Bi₂Te₃ 2D nanosheets were grown on Muscovite mica (V3 grade) substrates in the 1-inch diameter tube furnace. Optical microscope (Zeiss AxioLab A1) and AFM (Park XE 70) were used to characterize as-grown 2D nanosheets. More details about the growth can be found in the supporting information (SI). As-grown Bi₂Te₃ 2D nanosheets were immediately transferred to the pre-fabricated porous substrates using a thin film

of polymethyl methacrylate (PMMA, M.W. \sim 950,000, from MicroChem) as a sacrificial layer, and using a piece of polydimethylsiloxane (PDMS, Sylgard 184, Dow Corning) as the transfer carrier. A high 2D nanosheet transfer rate of $> 98\%$ can be routinely acquired, as shown in Figure S4. The bottleneck of our 2D nanosheet suspension process is the final drying procedure. Utilizing the supercritical fluid's extremely low surface tension, a promising suspension yield rate of $\sim 85\%$ has been achieved for 2D nanosheets ≥ 5 QLs. More details about the porous substrate fabrication and the transfer process are available in the SI.

In AFM based nano-indentations, AFM tips with soft cantilevers (DNP-10, from Bruker) were used to apply small point forces for generating vertical deflections of 2D nanosheets. AFM cantilever spring constant calibrations and AFM tip radius measurements are available in the SI.

Results and Discussion

Figure 1 presents the van der Waals epitaxial growth based on Li *et al.*'s report,²¹ and a process we developed specifically for transferring van der Waals epitaxy grown 2D nanosheets. On the mica substrate, the appearance of as-grown, identically-orientated equilateral triangle nanosheets was observed in the location corresponding to the upstream area of the tube furnace, and yet nanosheets with random morphologies were located in the downstream area. The distinct morphology *vs.* position dependency suggests that temperature and Bi_2Te_3 vapor pressure are both critical for controlling 2D nanosheet growth, which is in agreement with Li *et al.*'s report.²¹ Further, it is noticeable in **Figure 1(b)** that in the upstream area, 2D nanosheets in the majority have a triangular, larger morphology, and yet the minority are circular, smaller 2D nanosheets. This subtle morphology difference is owing to circular nanosheets were at an early growth stage, and triangular nanosheets had received a longer growth time. More detailed

morphology/size/thickness analysis from 59 nanosheets is included in the SI (see Figure S2) to further present the van der Waals epitaxy.

Figure 1(d) and **1(e)** are two representative 2D nanosheets before and after being transferred onto the pre-fabricated substrate with an array of circular holes. Distinctly, apparent reflectance colors of Bi₂Te₃ 2D nanosheets (under a white light illumination) have changed dramatically after the transfer or the suspension, which is ascribed to the combined effect of the silicon oxide thickness (270±3 nm), 2D nanosheet thicknesses (8 nm *vs.* 15 nm), and materials' refractive indices. Interestingly, colors of suspended regions are close to colors when these 2D nanosheets were still attached to the mica substrate, and yet colors of collapsed regions are close to the color of holes (the silicon oxide is 105±3 nm). The sharp optical color difference provides a simple, direct method for quickly determining nanosheet thicknesses and for identifying successfully-suspended 2D nanosheets, which is essentially the same principle for examining graphene²⁴ or MoS₂ 2D nanosheets.^{25, 26}

Figure 2 presents mechanical tests using the AFM based nano-indentation platform. The contact mode topography image (**Figure 2(b)**) shows that the circular 2D nanosheet (thickness ~ 5 nm, *i.e.*, 5 QLs) is successfully suspended over an array of holes (radius ~ 1 μm). It is evidenced by angles at the circular periphery that this 2D nanosheet was in the transition phase before forming a triangular morphology, which supports the earlier discussion regarding the nanosheet morphology difference. In **Figure 2(c)**, cross-sectional profiles (via contact mode) of the nanosheet across the center of the circular hole are displayed under different contact forces (0.02~2.95 nN). It is clearly shown that across the entire nanosheet suspension, resultant vertical deflections were proportional to forces applied by the AFM tip. More importantly, nanosheet deformations were reversible under forces applied.

To further examine the elastic properties, the AFM ramping mode (*i.e.*, force *vs.* distance mode) was used to apply point force loads (F , 0~18 nN) to the center of the suspended nanosheet. As illustrated in **Figure 2(d)**, the vertical deflection (δ) of the 2D nanosheet was obtained using its correlation with piezo-extension (ΔZ_{piezo}) and the cantilever deflection (ΔZ_c), $\delta = \Delta Z_{piezo} - \Delta Z_c$. **Figure 2(e)** shows three different sets of $F(\delta)$ curves with different maximum force loads, acquired from the same suspended nanosheet presented in **Figure 2(c)**. It is clearly shown that three $F(\delta)$ ramping curves are overlapped without any indication of a slippage or a rupture. Remarkably, a small force of only 15 nN was required to vertically deform the center of the suspended nanosheet by a displacement of ~100 nm, which implies the 2D nanosheet is quite mechanically compliant. We noticed that $F(\delta)$ responses acquired from the ramping mode (shown in **Figure 2(e)**) are inconsistent with $F(\delta)$ responses acquired from the contact mode (shown in **Figure 2(c)**), which is likely owing to a ramping mode solely causes a cantilever deflection but a contact mode contains both a cantilever deflection and tilt. Nevertheless, fully elastic deformation of Bi₂Te₃ 2D nanosheets is confirmed.

To find Bi₂Te₃ 2D nanosheet elastic properties, 26 samples including four different groups of thickness (7 samples for 5 QLs, 5 samples for 6 QLs, 8 samples for 8 QLs, and 6 samples for 14 QLs) were characterized, which provides the confidence of our analyses. All $F(\delta)$ curves of 26 samples are available in the SI (Figure S7, S8, S9 and S10). **Figure 2(f)** presents representative $F(\delta)$ curves for three groups of thickness: 5-QL, 8-QL, and 14-QL nanosheets, respectively. Interestingly, each group exhibits a distinctive $F(\delta)$ curve characteristic: 14-QL nanosheets show a linear $F(\delta)$ response because thick nanosheets behave as plates being bent. In contrast, the non-linear $F(\delta)$ curve of 5-QL nanosheets indicates a combined response from a bending behavior as plates and a stretching behavior as membranes.

The $F(\delta)$ behavior of the group of 8-QL nanosheets falls in between. Such thickness-dependent $F(\delta)$ characteristics were also found in mechanically-exfoliated MoS₂ 2D nanosheets,¹⁷ and could be understood using Komaragiri *et al.*'s model for a freestanding elastic circular film under point loads:²²

$$F = \left[\frac{4\pi E}{3(1-\nu^2)} \cdot \left(\frac{t^3}{r^2} \right) \right] \delta + (\pi T)\delta + \left(\frac{q^3 Et}{r^2} \right) \delta^3 . \quad (1)$$

Where E is the Young's modulus, t is the thickness of 2D nanosheet, r is the radius of the suspended circular nanosheet, ν is the Poisson's ratio for Bi₂Te₃ (~ 0.241),²⁷ T is the pretension of 2D nanosheet, and the dimensionless constant q equals $1/(1.05 - 0.15\nu - 0.16\nu^2)$. The first term is relevant to thick plates' bending behavior ($F \sim \delta$), the second term accounts for a pretensioning response ($F \sim \delta$), and the third term is relevant to thin membranes' non-linear stretching behavior ($F \sim \delta^3$). One might consider using Equation 1 to directly extract E and T , as commonly used for analyzing atomically thin, single layer 2D nanosheets.^{15, 16} We noticed that $F(\delta)$ curves of 5-QL nanosheets have a notable contribution from bending owing to $F(\delta)$ has not reached the membrane stretching regime in Komaragiri *et al.*'s model,²² and thus Equation 1 is inappropriate here for analyzing $F(\delta)$ curves of 5~14 QL nanosheets.

For analyzing thick 2D nanosheets, the alternative is to consider the limit of a small vertical deflection ($\delta \sim 0$),^{17, 23} which renders the third, non-linear term of Equation 1 negligible. The effective spring constant of 2D nanosheet (k_{2D}) could be derived from Equation 1, which gives:¹⁷

$$k_{2D} = \left. \frac{\partial F}{\partial \delta} \right|_{\delta \sim 0} = \frac{4\pi E}{3(1-\nu^2)} \cdot \left(\frac{t^3}{r^2} \right) + \pi T . \quad (2)$$

Figure 3 plots k_{2D} as a function of (t^3/r^2) for all 26 samples, while all k_{2D} values can be found in the SI. Clearly, a good linear fit using Equation 2 is obtained. Note that the slightly curved

suspension surfaces are considered for acquiring the radii of the suspended circular nanosheets, and they are compared with the holes' radii for determining E and T . The resultant differences in E and T are actually negligible in comparison with the combined errors induced by the AFM measurements of the 2D nanosheet thicknesses, the hole radii, and the point forces (*i.e.*, errors from cantilever spring constant). We took the lower limit and the upper limit from the deviation of the linear fit, and consequently $E = 11.7\sim 25.7$ GPa and $T = 0.011\sim 0.028$ N/m were found. Using Equation 2 to analyze these samples, both E and T are assumed to be independent of thickness and sample,¹⁷ which is considered as the uncertainty to the acquired E and T . Because $F(\delta)$ curves of 5-QL nanosheets have not reached the membrane stretching regime,²² and it is argued that E and T are thickness-independent in the range of 5~14 QLs. In addition, among 5~14 QL nanosheets, k_{2D} values of each group are from the same 2D nanosheet (*i.e.*, same crystal quality), and 2D nanosheets for all four groups are from the same mica substrate (*i.e.*, same growth batch) and from the same transfer step (*i.e.*, a similar degree of pretensioning), which presumably mitigate the uncertainty of our analysis.

Using the extracted E (averaged, ~ 18.7 GPa) and the measured r_{tip} (averaged, ~ 26.8 nm, see Figure S6), one could estimate the in-plane stress exerted by the tip at the central, protruding part of the 2D nanosheet.^{15, 16} In Bhatia *et al.*'s model, the stress is expressed as:²⁸

$$\sigma_{applied}^{2D} = \sqrt{\frac{F_{applied} E^{2D}}{4\pi r_{tip}}} \quad (3)$$

Where $E^{2D} = E \cdot t$ is the 2D modulus. For a normal force of 15 nN (*i.e.*, within the elastic range) applied to the 5-QL nanosheet (see **Figure 2(e)**), $\sigma_{applied}^{2D}$ yields 2.0 ± 0.4 N/m, corresponding to 0.40 ± 0.08 GPa for the 5-QL nanosheet under the specific elastic stretching state, *i.e.*, 2~3 % strain. Without a rupture using the maximum force that could be applied by our AFM platform,

we expect that a larger breaking strain (*i.e.*, > 3%) can be obtained for the Bi₂Te₃ 2D nanosheets. Meanwhile, the pretension (0.011~0.028 N/m) is presumably owing to possible crystal defects and the suspension. As shown in **Figure 2(c)**, the suspended surface profile (with $F=0.02$ nN) of the 5-QL nanosheet evidences the nanosheet attachment at the hole's sidewall, which is 3~5 nm in depth around the periphery of the hole. Similar sidewall attachment is also commonly observed in suspensions of other 2D nanosheet samples, which would contribute to the nanosheet pretension to a varied extent.^{15, 16}

The Young's modulus of Bi₂Te₃ 2D nanosheets extracted from the linear regime ($\delta \sim 0$) was found to be significantly decreased, surprisingly being only 22~49 % of Bi₂Te₃ bulk in-plane Young's modulus (50~55 GPa at room temperature).^{29, 30} **Table 1** summarizes Young's moduli of van der Waals family 2D nanosheets^{15-19, 23, 31, 32} and bulk samples.³³⁻³⁷ In comparison with other van der Waals family 2D nanosheets, multi-QL Bi₂Te₃ 2D nanosheets have an extremely small Young's modulus (yet larger than that of the flakes of metal organic frameworks, MOFs³⁸), and yet show remarkable, robust elastic behaviors. The reduction of Young's modulus may be attributed to crystal defects, since antisites and/or vacancies could be formed in Bi₂Te₃ crystal during the van der Waals epitaxy. Similar reductions of Young's modulus were also observed in defective monolayer graphene sheets (E increases first then decreases with the defect density)³⁹ and defective 2~5 layered boron nitride 2D nanosheets.³² The defect-dependent crack propagation in the defective graphene monolayers was also investigated by the AFM nano-indentations.⁴⁰ Without crystal defects, theoretically calculated moduli of graphene and boron nitride monolayers are comparable to their bulk counterparts,⁴¹ which is indeed consistent with the experimental work on pristine graphene.¹⁵ Another possibility of the Young's modulus reduction is the size effect as observed in Si nanofilms,^{42, 43}

because surface relaxation and surface energy may play a role in 5~14 QL Bi_2Te_3 2D nanosheets.⁴⁴

It is also noticeable in **Table 1** that 2D nanosheets of transition metal dichalcogenide have Young's moduli larger than their bulk values. For example, multi-layered MoS_2 nanosheets have Young's moduli comparable with the bulk counterpart. Strikingly, Young's modulus of monolayer MoS_2 is larger than that of multi-layered MoS_2 .^{16-19, 34} The increase in Young's modulus from multi-layered MoS_2 to monolayer MoS_2 is ascribed to a reduced contribution of interlayer sliding or stacking defects.^{17, 19} Yet, this factor may not be applied for Bi_2Te_3 2D nanosheets owing to the Young's modulus reduction from its bulk value. Limited by the yield of our 2D nanosheet transfer, Bi_2Te_3 2D nanosheets with 4-QL or less could not be characterized in this work, and thus it is still uncertain whether 1-QL Bi_2Te_3 2D nanosheets have a Young's modulus comparable to its bulk value, as shown by graphene.¹⁵ Future works of elastic properties of 1~4 QL Bi_2Te_3 2D nanosheets will help elucidate the fundamental understanding of their elastic properties, and further help enrich the knowledge of mechanical properties of van der Waals family 2D nanosheets.

Conclusions

In summary, van der Waals epitaxy grown Bi_2Te_3 2D nanosheets were successfully detached from mica substrates and suspended over an array of holes, allowing mechanical properties to be tested for the first time via AFM based nano-indentations. Elastic behaviors of Bi_2Te_3 2D nanosheets were confirmed to be robust during nano-indentation tests. The averaged Young's modulus among 5~14 QL nanosheets is much less than that of bulk Bi_2Te_3 , and also significantly less than other van der Waals family 2D nanosheets, such as graphene, MoS_2 , WS_2 , h-boron nitride, and mica. The elastic properties of 5~14 nm-thick Bi_2Te_3 nanosheets are of

interest for the TSS research, because TSSs would hybridize when the thickness of a TI film is thinner than TSSs' penetration depth (*i.e.*, 5 nm for Bi_2Te_3).^{6, 7} The significantly enhanced compliant properties of TI-based 2D nanosheets suggest the likelihood of elastic strain engineering of TSSs towards practical applications.

Acknowledgements

This work at the University of Alabama (UA) was supported by the start-up fund (Wang, 2011). L. Guo would like to acknowledge UA MINT Graduate Student Scholarships supporting her study at UA in 2013 and 2014. Q. Moore would like to acknowledge the NSF-REU Program (EEC-1358750). Authors acknowledge instrumental supports from UA Microfabrication Facility, UA Central Analytical Facility, UA MINT Center, and UA Optical Analysis Facility.

Additional information

Supporting Information is submitted with this manuscript.

Figures and Figure Captions:

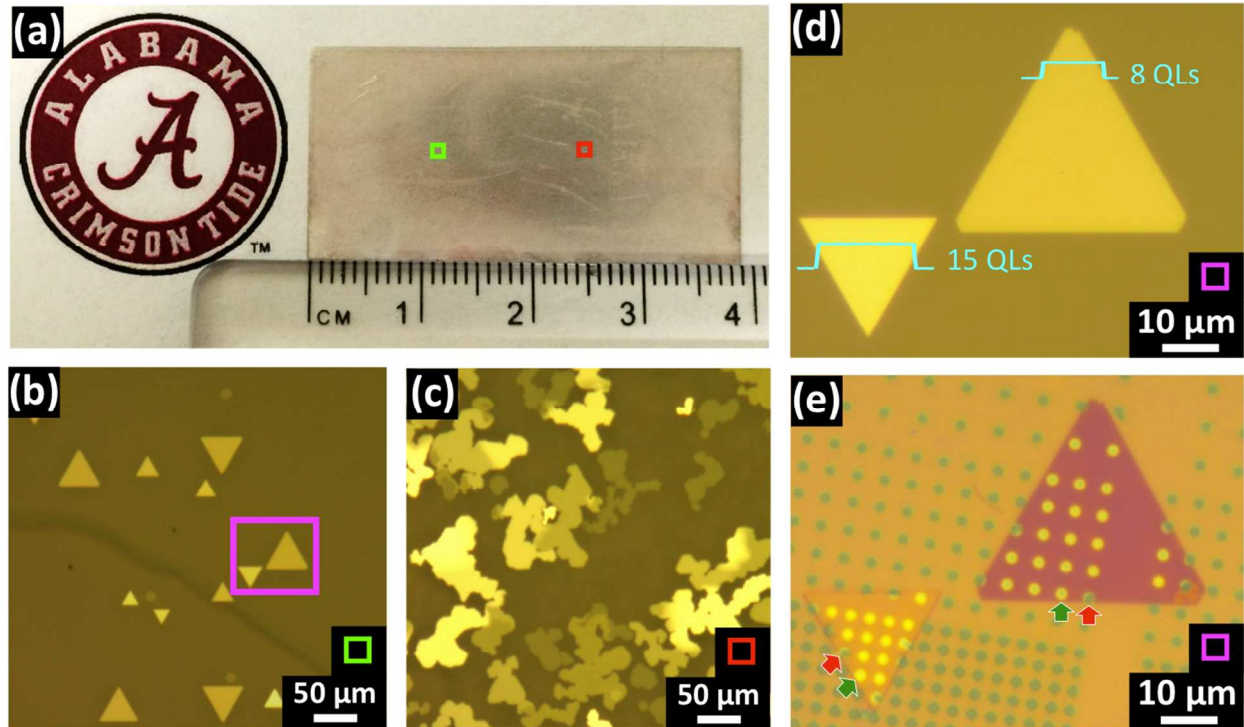


Figure 1. Bi_2Te_3 2D nanosheets prepared by the van der Waals epitaxy, and their transfer to the porous substrate. (a) Photograph of the mica substrate ($\sim 2 \times 4$ cm) after a typical growth. The deposition area shows a grayish color. The upstream and the downstream area are marked respectively by a green square and a red square, and their optical images are shown in (b) and (c), respectively. (d) Optical image of two representative Bi_2Te_3 2D nanosheets, identical to ones labeled by the pink rectangle in (b). Insets are AFM cross-sectional profiles (cyan) showing the quantities of quintuple layer stacking. (e) Optical image of two representative Bi_2Te_3 2D nanosheets after being transferred. Optical colors of suspended regions (labeled by green arrows) are clearly different from colors of supported regions, and also very different from colors at collapsed regions (labeled by red arrows).

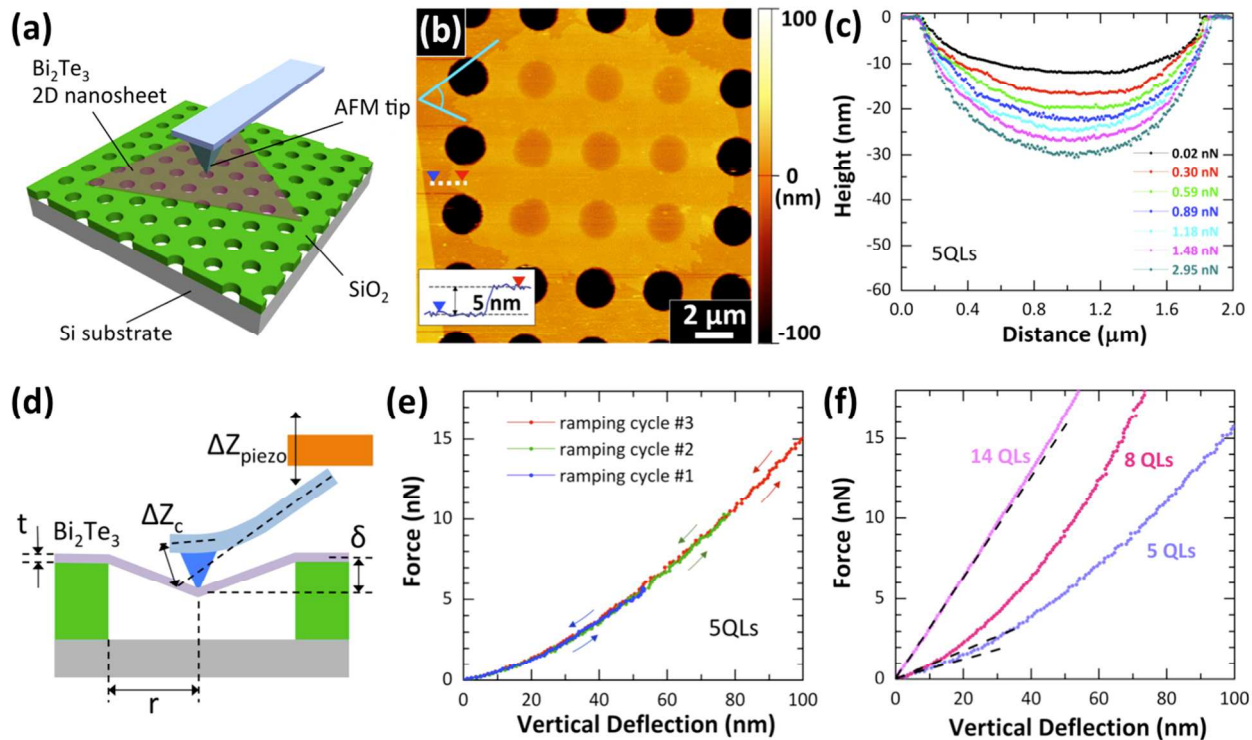


Figure 2. Bi_2Te_3 2D nanosheet elastic measurements using the AFM platform. **(a)** Schematic showing a triangular 2D nanosheet covering an array of holes, and one suspended circular nanosheet being probed by an AFM tip. **(b)** AFM topography image (contact mode, $F = 0.02$ nN) of the transferred, circular 2D nanosheet. The 60° angle mark (cyan) depicts the transient growth toward a triangular morphology. Inset is the cross-sectional profile indicating the 2D nanosheet thickness = 5 ± 0.5 nm, *i.e.*, 5 QLs. **(c)** Contact mode, cross-sectional profiles across the center of the circular hole covered by the 5-QL nanosheet (the upper/left one in **(b)**). Contact forces, ranging from 0.02 to 2.95 nN, were applied to the suspended circular nanosheet. **(d)** Schematic of the AFM based nano-indentation test for acquiring $F(\delta)$ behaviors. **(e)** $F(\delta)$ curves of three different ramping cycles, which were acquired using the same suspended nanosheet presented in **(c)**. **(f)** Representative $F(\delta)$ curves of 5 QLs, 8 QLs, and 14 QLs with linear fittings at $\delta \sim 0$ (black dash lines) for acquiring k_{2D} .

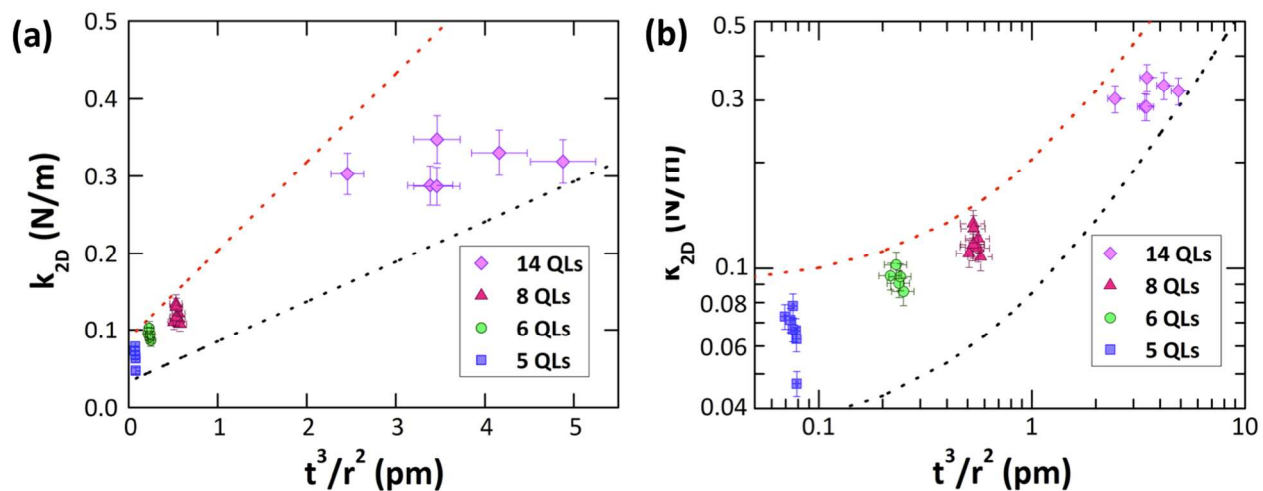


Figure 3. Plots of k_{2D} vs. (t^3/r^2) in the (a) linear and (b) logarithmic scale, consisting of 26 samples in total. The linear fitting was performed, resulting a deviation comprising the upper (red dot line) and the lower limit (black dot line). Error bars for all 26 samples in the x -axis are based on the AFM measurement errors on the 2D nanosheet thicknesses and suspended circular nanosheet radii, while error bars in the y -axis are mainly due to AFM cantilever spring constant calibration errors (available in the SI).

Table 1. Young's moduli of van der Waals family 2D nanosheets acquired by AFM nano-indentations, which were extracted either in the $F \sim \delta$ regime (labeled by #) or the $F \sim \delta^3$ regime. Bulk Young's moduli and theoretical predictions (labeled by *) are also included.

Van der Waals 2D materials	# of Monolayers	Young's Modulus (GPa)	Reference
Bi₂Te₃	5~14 (F~ δ)	18.7 ± 7.0 #	This work
	3~15	$37 \sim 53$ *	Y. Tong <i>et al.</i> ⁴⁴
	Bulk (in-plane)	54.2	J. Jenkins <i>et al.</i> ²⁹
	Bulk (in-plane)	51.4 *	B. Huang and M. Kaviani ³⁰
Graphene	1	1000 ± 100	C. Lee <i>et al.</i> ¹⁵
	1	1029 *	Kudin <i>et al.</i> ⁴¹
	Bulk	1020 ± 30	O. L. Blakslee <i>et al.</i> ³³
Graphene Oxide	1	207.6 ± 23.4	J. Suk <i>et al.</i> ³¹
	2	223.9 ± 17.7	
	3	229.5 ± 27.0	
MoS₂	1	270 ± 100	S. Bertolazzi <i>et al.</i> ¹⁶
	2	200 ± 60	
	5~25	330 ± 70 #	A. Castellanos-Gomez <i>et al.</i> ¹⁷
	1	264 ± 18	K. Liu <i>et al.</i> ¹⁹
	2	228 ± 16	
	1	195 ± 49	R. Cooper <i>et al.</i> ¹⁸
Bulk	238	J. Feldman ³⁴	
WS₂	1	272 ± 18	K. Liu <i>et al.</i> ¹⁹
	Bulk	150	Sourisseau <i>et al.</i> ³⁵
h-Boron Nitride	2~5	233 ± 32	L. Song <i>et al.</i> ³²
	1	810 *	Kudin <i>et al.</i> ⁴¹
	Bulk	811	Bosak <i>et al.</i> ³⁶
Mica	2~14	202 ± 22 #	A. Castellanos-Gomez <i>et al.</i> ²³
	Bulk	176.5 ± 1.1	L. McNeil and M. Grimsditch ³⁷
MOFs	1~50	5 ± 0.5	C. Hermosa <i>et al.</i> ³⁸

References:

1. Y. L. Chen, J. G. Analytis, J. H. Chu, Z. K. Liu, S. K. Mo, X. L. Qi, H. J. Zhang, D. H. Lu, X. Dai, Z. Fang, S. C. Zhang, I. R. Fisher, Z. Hussain and Z. X. Shen, *Science*, 2009, **325**, 178-181.
2. H. J. Zhang, C. X. Liu, X. L. Qi, X. Dai, Z. Fang and S. C. Zhang, *Nature Physics*, 2009, **5**, 438-442.
3. M. Z. Hasan and J. E. Moore, *Annual Review of Condensed Matter Physics*, 2011, **2**, 55-78.
4. K. S. Novoselov, A. K. Geim, S. V. Morozov, D. Jiang, M. I. Katsnelson, I. V. Grigorieva, S. V. Dubonos and A. A. Firsov, *Nature*, 2005, **438**, 197-200.
5. D. Kong and Y. Cui, *Nature Chemistry*, 2011, **3**, 845-849.
6. C.-X. Liu, H. Zhang, B. Yan, X.-L. Qi, T. Frauenheim, X. Dai, Z. Fang and S.-C. Zhang, *Physical Review B*, 2010, **81**, 041307.
7. Y. Zhang, K. He, C.-Z. Chang, C.-L. Song, L.-L. Wang, X. Chen, J.-F. Jia, Z. Fang, X. Dai, W.-Y. Shan, S.-Q. Shen, Q. Niu, X.-L. Qi, S.-C. Zhang, X.-C. Ma and Q.-K. Xue, *Nature Physics*, 2010, **6**, 584-588.
8. S. M. Young, S. Chowdhury, E. J. Walter, E. J. Mele, C. L. Kane and A. M. Rappe, *Physical Review B*, 2011, **84**, 085106.
9. W. Liu, X. Peng, C. Tang, L. Sun, K. Zhang and J. Zhong, *Physical Review B*, 2011, **84**, 245105.
10. J. Hicks, A. Tejada, A. Taleb-Ibrahimi, M. S. Nevius, F. Wang, K. Shepperd, J. Palmer, F. Bertran, P. Le Fevre, J. Kunc, W. A. de Heer, C. Berger and E. H. Conrad, *Nature Physics*, 2013, **9**, 49-54.
11. F. Guinea, M. I. Katsnelson and A. K. Geim, *Nature Physics*, 2010, **6**, 30-33.
12. C. Chen, J. Z. Wu, K. T. Lam, G. Hong, M. Gong, B. Zhang, Y. Lu, A. L. Antaris, S. Diao, J. Guo and H. Dai, *Advanced Materials*, 2014, 303-309.
13. A. Castellanos-Gomez, R. Roldán, E. Cappelluti, M. Buscema, F. Guinea, H. S. J. van der Zant and G. A. Steele, *Nano Letters*, 2013, **13**, 5361-5366.
14. H. J. Conley, B. Wang, J. I. Ziegler, R. F. Haglund, S. T. Pantelides and K. I. Bolotin, *Nano Letters*, 2013, **13**, 3626-3630.
15. C. Lee, X. Wei, J. W. Kysar and J. Hone, *Science*, 2008, **321**, 385-388.
16. S. Bertolazzi, J. Brivio and A. Kis, *ACS Nano*, 2011, **5**, 9703-9709.
17. A. Castellanos-Gomez, M. Poot, G. A. Steele, H. S. J. van der Zant, N. Agrait and G. Rubio-Bollinger, *Advanced Materials*, 2012, **24**, 772-775.
18. R. Cooper, C. Lee, C. Marianetti, X. Wei, J. Hone and J. Kysar, *Physical Review B*, 2013, **87**, 035423.
19. K. Liu, Q. Yan, M. Chen, W. Fan, Y. Sun, J. Suh, D. Fu, S. Lee, J. Zhou, S. Tongay, J. Ji, J. B. Neaton and J. Wu, *Nano Letters*, 2014, **14**, 5097-5103.
20. V. Nicolosi, M. Chhowalla, M. G. Kanatzidis, M. S. Strano and J. N. Coleman, *Science*, 2013, **340**, 1226419.
21. H. Li, J. Cao, W. Zheng, Y. Chen, D. Wu, W. Dang, K. Wang, H. Peng and Z. Liu, *Journal of the American Chemical Society*, 2012, **134**, 6132-6135.
22. U. Komaragiri, M. R. Begley and J. G. Simmonds, *Journal of Applied Mechanics*, 2005, **72**, 203-212.

23. A. Castellanos-Gomez, M. Poot, A. Amor-Amorós, G. Steele, H. J. van der Zant, N. Agrait and G. Rubio-Bollinger, *Nano Res.*, 2012, **5**, 550-557.
24. P. Blake, E. W. Hill, A. H. Castro Neto, K. S. Novoselov, D. Jiang, R. Yang, T. J. Booth and A. K. Geim, *Applied Physics Letters*, 2007, **91**, 063124.
25. A. Castellanos-Gomez, N. Agrait and G. Rubio-Bollinger, *Applied Physics Letters*, 2010, **96**, 213116.
26. A. Castellanos-Gomez, M. Poot, G. Steele, H. van der Zant, N. Agrait and G. Rubio-Bollinger, *Nanoscale Research Letters*, 2012, **7**, 233.
27. H. Koc, A. M. Mamedov and E. Ozbay, 2013.
28. N. M. Bhatia and W. Nachbar, *International Journal of Non-Linear Mechanics*, 1968, **3**, 307-324.
29. J. O. Jenkins, J. A. Rayne and R. W. Ure, *Physical Review B*, 1972, **5**, 3171-3184.
30. B.-L. Huang and M. Kaviani, *Physical Review B*, 2008, **77**, 125209.
31. J. W. Suk, R. D. Piner, J. An and R. S. Ruoff, *ACS Nano*, 2010, **4**, 6557-6564.
32. L. Song, L. Ci, H. Lu, P. B. Sorokin, C. Jin, J. Ni, A. G. Kvashnin, D. G. Kvashnin, J. Lou, B. I. Yakobson and P. M. Ajayan, *Nano Letters*, 2010, **10**, 3209-3215.
33. O. L. Blakslee, D. G. Proctor, E. J. Seldin, G. B. Spence and T. Weng, *Journal of Applied Physics*, 1970, **41**, 3373-3382.
34. J. L. Feldman, *Journal of Physics and Chemistry of Solids*, 1976, **37**, 1141-1144.
35. C. Sourisseau, M. Fouassier, M. Alba, A. Ghorayeb and O. Gorochov, *Materials Science and Engineering: B*, 1989, **3**, 119-123.
36. A. Bosak, J. Serrano, M. Krisch, K. Watanabe, T. Taniguchi and H. Kanda, *Physical Review B*, 2006, **73**, 041402.
37. L. E. McNeil and M. Grimsditch, *Journal of Physics: Condensed Matter*, 1993, **5**, 1681.
38. C. Hermosa, B. R. Horrocks, J. I. Martinez, F. Liscio, J. Gomez-Herrero and F. Zamora, *Chemical Science*, 2015, **6**, 2553-2558.
39. G. López-Polín, C. Gómez-Navarro, V. Parente, F. Guinea, M. I. Katsnelson, F. Perez-Murano and J. Gómez-Herrero, *Nature Physics*, 2015, **11**, 26-31.
40. G. López-Polín, J. Gómez-Herrero and C. Gómez-Navarro, *Nano Letters*, 2015, **15**, 2050-2054.
41. K. N. Kudin, G. E. Scuseria and B. I. Yakobson, *Physical Review B*, 2001, **64**, 235406.
42. A. I. Fedorchenko, A.-B. Wang and H. H. Cheng, *Applied Physics Letters*, 2009, **94**, 152111.
43. X. Li, T. Ono, Y. Wang and M. Esashi, *Applied Physics Letters*, 2003, **83**, 3081-3083.
44. Y. Tong, F. Yi, L. Liu, P. Zhai and Q. Zhang, *Physica B: Condensed Matter*, 2010, **405**, 3190-3194.